

# Chapter 2

## AB<sub>2</sub>O<sub>4</sub> Compounds at High Pressures

Daniel Errandonea

**Abstract** In this chapter, we present an overview of the effects of pressure on the crystalline structure and physical properties of oxygen-based spinels and other related oxides. Recent X-ray diffraction and Raman spectroscopy studies are summarized. A brief description of pressure-driven transitions and post-spinel structures is also provided. We also compare the response to high-pressure of several spinel oxides. We conclude with an examination of elastic and magnetic properties.

**Keywords** Spinel · Post-spinel · Phase transition · Crystal structure · Lattice vibrations · Elastic properties

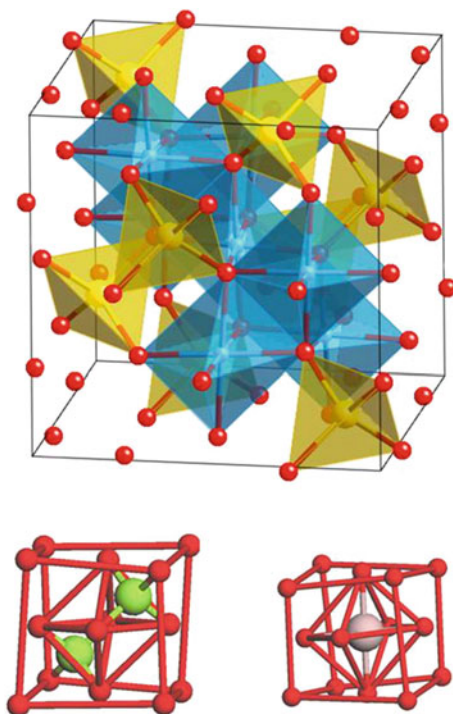
### 2.1 Introduction

Many compounds of the AB<sub>2</sub>X<sub>4</sub> family, in particular oxides (X = O), crystallize at ambient conditions in the spinel structure. Spinel is the magnesium aluminum oxide member of this large group of materials. It has the formula MgAl<sub>2</sub>O<sub>4</sub> and gives its name to the family of compounds that share the same structural arrangement. Consequently, here we will name as spinel to any material of general formulation AB<sub>2</sub>X<sub>4</sub> which crystallizes in the cubic (isometric) crystal system with space group *Fd* $\bar{3}m$  (No. 227). In this structure, shown in Fig. 2.1, the X anions are located at (*u*, *u*, *u*), Wyckoff position 32e, with *u*  $\approx$  0.25. They are arranged in a cubic close-packed lattice. In addition, the cations A and B occupy in the lattice respectively tetrahedral (1/8, 1/8, 1/8) sites, Wyckoff position 8a, and octahedral (1/2, 1/2, 1/2) sites, Wyckoff position 16d. Therefore, the single positional parameter *u* plus the unit-cell parameter *a* are sufficient to determine the spinel structure.

---

D. Errandonea (✉)  
Universitat de Valencia, Valencia, Spain  
e-mail: daniel.errandonea@uv.es

**Fig. 2.1** Schematic view of the spinel structure with octahedral (blue) and tetrahedral units (yellow). Oxygen atoms are represented in red. In the lower part the tetrahedral (left) and octahedral (right) coordination of cations is represented. Drawings made using crystal maker



In spinels, A and B can be divalent, trivalent, or tetravalent cations, including magnesium, zinc, iron, manganese, aluminum, chromium, gallium, titanium, and silicon among other elements of the Periodic Table. Although the anion is normally oxygen (oxospinel), it can be also a chalcogen element, like S (thiospinels) or Se (selenospinel). Spinel can either be synthesized in the laboratory or in some cases occur as minerals. Some of the principal members of the oxide spinel family are: spinel ( $\text{MgAl}_2\text{O}_4$ ), gahnite ( $\text{ZnAl}_2\text{O}_4$ ), hercynite ( $\text{FeAl}_2\text{O}_4$ ), cuprospinel ( $\text{CuFe}_2\text{O}_4$ ), magnetite ( $\text{Fe}_3\text{O}_4$ ), ulvöspinel ( $\text{TiFe}_2\text{O}_4$ ), chromite ( $\text{FeCr}_2\text{O}_4$ ), magnesiochromite ( $\text{MgCr}_2\text{O}_4$ ), galaxite ( $\text{MnAl}_2\text{O}_4$ ), magnesioferrite ( $\text{MgFe}_2\text{O}_4$ ), franklinite ( $\text{ZnFe}_2\text{O}_4$ ), trevorite ( $\text{NiFe}_2\text{O}_4$ ), and the high-pressure silicate ringwoodite [ $(\text{Mg}, \text{Fe})_2\text{SiO}_4$ ]. Spinel is usually ordered (A and B in tetrahedral and octahedral sites, respectively) and they are referred as “normal” spinels, but mutual substitution of A and B cations has been reported in many materials. The extreme cases of cation substitution lead to “inverse” spinels such as  $\text{CoFe}_2\text{O}_4$ , where the Co cation occupies one half of the octahedral sites and the Fe cation occupies all the tetrahedral sites. In general, most spinels have some degree of inversion. A particular case is  $\text{NiAl}_2\text{O}_4$ . In this oxide a complete randomization of both cations in octahedral and tetrahedral sites is observed.

After Finger et al. [1] studied the structure of spinel and magnetite under compression up to 4 GPa, many high-pressure studies have been performed in spinels.

The main interest to study these materials comes from geophysics, but also from technological applications and fundamental physics. In particular, spinel oxides have been extensively studied under pressure because they are constituents of many igneous and metamorphic rocks. Also because of the fact that the 660 km seismic discontinuity in the Earth's mantle has long been identified with the decomposition of ringwoodite into (Mg, Fe)SiO<sub>3</sub> perovskite and (Mg, Fe)O magnesiowüstite [2].

In this chapter we will review different high-pressure studies on spinel-structured oxides. We will mainly focus on X-ray diffraction and Raman studies since the pressure behavior of oxospinel has been mostly studied with these two techniques. We will describe the effects of pressure in the spinel structure discussing facts like bulk and polyhedral compressibility, cation size, and cation substitution. We will also comment on pressure-induced phase transitions and on the different post-spinel structures. In particular, zinc gallate (ZnGa<sub>2</sub>O<sub>4</sub>) will be used as a test model. A comprehensive review on high-pressure effects on spinel oxides was published more than a decade ago by Smyth [3], but recently a lot of progress has been done in the understanding of the behavior of spinels at high pressures. Therefore, we think it is timely to include a section devoted them here.

## 2.2 Isothermal Compression of the Spinel Phase: X-ray Diffraction Studies

The effect of pressure on the lattice parameter, hence the volume, for different spinels has been determined at room temperature by means of powder X-ray diffraction measurements employing diamond-anvil cells. These experiments show that in most spinel oxides, the diffraction patterns can be indexed with the cubic spinel structure up to around 30 GPa. At higher pressures, phase transitions to different post-spinel structures take place. In contrast with oxide spinels, in sulfide and selenide spinels the pressure range of stability is smaller, being transition pressures smaller than 15 GPa, as will be discussed in the next chapter. A summary of transition pressures in spinel oxides is given in Table 2.1 [4–17]. From the refinements of X-ray diffraction patterns collected under compression, the evolution of the unit-cell parameters and atomic positions can be obtained as a function of pressure.

Figure 2.2 shows the pressure dependence of the volume for the spinel phase of ZnGa<sub>2</sub>O<sub>4</sub>, MgCr<sub>2</sub>O<sub>4</sub>, MgAl<sub>2</sub>O<sub>4</sub>, and the natural chromium spinel (NaMgFeTi)<sub>0.9661</sub>(CrAl)<sub>2.0241</sub>O<sub>4</sub>. As can be seen in the figure, ZnGa<sub>2</sub>O<sub>4</sub> is the less compressible material of all of them. A fit to the ZnGa<sub>2</sub>O<sub>4</sub> data with a third-order Birch–Murnaghan equation of state (EOS) [19] gives:  $V_0 = 580.1(9) \text{ \AA}^3$ ,  $B_0 = 233(8) \text{ GPa}$ , and  $B'_0 = 8.3(4)$ , where  $V_0$ ,  $B_0$ , and  $B'_0$  are the zero-pressure volume, bulk modulus, and its pressure derivative, respectively. According to this result, ZnGa<sub>2</sub>O<sub>4</sub> is the most incompressible among the studied oxide spinels up to now. The bulk modulus of different oxide spinels is summarized in Table 2.2 [4, 8–10, 14, 15, 20–30]. As can be observed in Table 2.2, sulfide and selenide spinels are much more compressible than oxide spinels.

**Table 2.1** Transition pressures ( $P_t$ ) and high-pressure phases of different spinels (space groups are indicated for HP phases when known)

Compound	$P_t$ (GPa)	HP phase	Reference	Compound	$P_t$ (GPa)	HP phase	Reference
ZnGa <sub>2</sub> O <sub>4</sub>	31.2	<i>I4<sub>1</sub>/amd</i>	[4]	ZnCr <sub>2</sub> O <sub>4</sub>	17–35	unknown	[11]
	55	<i>Pnma</i>					
(Mg, Fe) <sub>2</sub> SiO <sub>4</sub>	24	(Mg,Fe)SiO <sub>3</sub> + (Mg,Fe)O	[5]	Fe <sub>3</sub> O <sub>4</sub>	24	<i>Pbcm</i>	[12]
MgAl <sub>2</sub> O <sub>4</sub>	25	<i>Pnma</i>	[6]	ZnCr <sub>2</sub> S <sub>4</sub>	10	amorphization	[13]
	40	<i>Cmcm</i>					
MgFe <sub>2</sub> O <sub>4</sub>	27.7	unknown	[7]	ZnTi <sub>2</sub> O <sub>4</sub>	24–32	<i>Cmcm</i>	[18]
NiMn <sub>2</sub> O <sub>4</sub>	12	<i>I4<sub>1</sub>/amd</i>	[8]	MgIn <sub>2</sub> S <sub>4</sub>	9.8	<i>Fd<math>\bar{3}</math>m</i>	[14]
ZnFe <sub>2</sub> O <sub>4</sub>	25	unknown	[9]	CdIn <sub>2</sub> S <sub>4</sub>	9.3	<i>Fd<math>\bar{3}</math>m</i>	[14]
CoFe <sub>2</sub> O <sub>4</sub>	27	unknown	[9]	MnIn <sub>2</sub> S <sub>4</sub>	6.8	<i>Fd<math>\bar{3}</math>m</i>	[14]
MgFe <sub>2</sub> O <sub>4</sub>	30	unknown	[9]	FeCr <sub>2</sub> S <sub>4</sub>	9	<i>I<sub>2</sub>/m</i>	[15]
MgCr <sub>2</sub> O <sub>4</sub>	20	<i>I4<sub>1</sub>/amd</i>	[10]	CuIr <sub>2</sub> S <sub>4</sub>	4	unknown	[16]
				CuIr <sub>2</sub> Se <sub>4</sub>	2.6	unknown	[17]

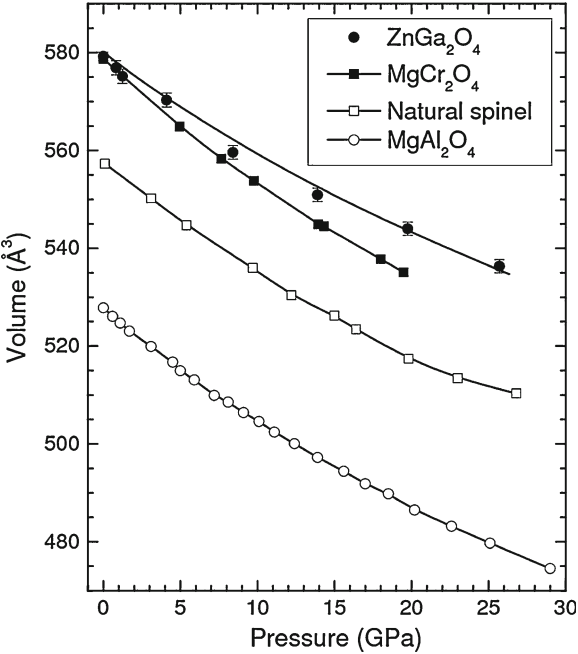


**Fig. 2.2** Pressure dependence of the unit-cell volume of different spinel oxides. Data taken from [4, 10, 24, 27]

**Table 2.2** Comparison of experimentally-determined bulk moduli of different oxide spinels

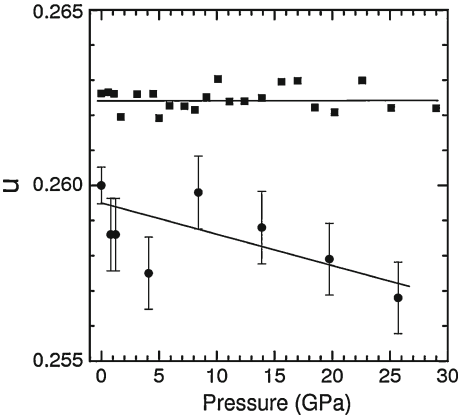
Compound	B <sub>0</sub> (GPa)	B' <sub>0</sub>	Reference	Compound	B <sub>0</sub> (GPa)	B' <sub>0</sub>	Reference
ZnGa <sub>2</sub> O <sub>4</sub>	233	8.3	[4]	MgAl <sub>2</sub> O <sub>4</sub>	194–212	4–5.6	[27, 28]
ZnAl <sub>2</sub> O <sub>4</sub>	201–211	4.8–7.6	[9, 20]	MgFe <sub>2</sub> O <sub>4</sub>	179–181	3.3–6.3	[9, 21]
ZnCr <sub>2</sub> O <sub>4</sub>	183	7.9	[21]	MgCr <sub>2</sub> O <sub>4</sub>	189	7.2	[10]
ZnFe <sub>2</sub> O <sub>4</sub>	166–185	3.1–9.3	[22]	Mg <sub>2</sub> SiO <sub>4</sub>	184	4	[28]
ZnMn <sub>2</sub> O <sub>4</sub>	183	4	[23]	CoFe <sub>2</sub> O <sub>4</sub>	179	3.7	[9]
ZnMn <sub>2</sub> O <sub>4</sub>	162	4	[18]	NiMn <sub>2</sub> O <sub>4</sub>	206	4	[8]
Natural chromiumspinel	209	7	[24]	Ni <sub>2</sub> SiO <sub>4</sub>	220	4	[27]
Fe <sub>2</sub> SiO <sub>4</sub>	188	5.5	[25]	CuMn <sub>2</sub> O <sub>4</sub>	198	4	[29]
Fe <sub>3</sub> O <sub>4</sub>	183–192	4–5.6	[26]	CdIn <sub>2</sub> S <sub>4</sub>	79.8	3.1	[14]
FeCr <sub>2</sub> S <sub>4</sub>	85.4	4	[14]	MgIn <sub>2</sub> S <sub>4</sub>	76	2.8	[14]
CdCr <sub>2</sub> Se <sub>4</sub>	101	5.2	[30]	MnIn <sub>2</sub> S <sub>4</sub>	78	3.2	[15]
CdGa <sub>2</sub> Se <sub>4</sub>	48	4.8	[30]				

ZnGa<sub>2</sub>O<sub>4</sub> is apparently the less compressible compound among them. The pressure derivative of the bulk modulus is also included for completeness. Sulphur and selenium spinels (to be discussed in next chapter) are included here to facilitate comparison

An interesting fact to note here, it is that apparently, cation inversion could cause a change of the compressibility of spinels. Evidence of such pressure-induced cation inversion has been found in other oxide spinels upon compression; e.g. NiAl<sub>2</sub>O<sub>4</sub> [31]. In particular, compressibilities for normal (fully ordered) versus inverse (with disordered octahedral cations) variants were shown to differ by as much as 17 % [28].

From the data collected for ZnGa<sub>2</sub>O<sub>4</sub> it was also deduced a negative pressure coefficient of the parameter  $u$  under compression. This tendency indicates that zinc gallate tries to reach the ideal structure ( $u = 0.25$ ) when pressurized. The pressure dependence of  $u$  is shown in the inset on Fig. 2.3. A similar behavior was observed in other cubic spinels like ZnAl<sub>2</sub>O<sub>4</sub> [20]. Ab initio calculations predict a similar behavior for ZnAl<sub>2</sub>O<sub>4</sub> and ZnIn<sub>2</sub>O<sub>4</sub> [32]. The oxygen  $u$  parameter in spinels reflects

**Fig. 2.3** Pressure dependence of the oxygen parameter  $u$  for ZnGa<sub>2</sub>O<sub>4</sub> [4] (circles) and Fe<sub>2</sub>SiO<sub>4</sub> [33] (squares)



the relative size of A and B cations in their respective tetrahedral and octahedral sites. Thus, their behavior under compression is determined by the relative compressibility of these two polyhedral units. Difference in octahedral and polyhedral compression may lead to different behaviors of  $u$  with pressure. In particular, it can be seen in Fig. 2.3 that in  $\text{Fe}_2\text{SiO}_4$  [33]  $u$  remains nearly constant up to 30 GPa. In order to illustrate better the influence of pressure on  $u$ , it is instructive the comparison made by Finger et al. [26] of the high-pressure behavior of this parameter in  $\text{MgAl}_2\text{O}_4$ ,  $\text{Fe}_3\text{O}_4$ , and  $\text{Ni}_2\text{SiO}_4$ . The  $u$  parameter of  $\text{MgAl}_2\text{O}_4$  decreases with pressure, this indicating that  $\text{MgO}_4$  tetrahedra compress more than the  $\text{AlO}_6$  octahedra. On the other hand, the  $u$  parameter is not affected by pressure in  $\text{Fe}_3\text{O}_4$  since Fe–O are equally compressible in both tetrahedral and octahedral units, and therefore the spinel structure simply scales with pressure. Finally,  $u$  increases upon compression in  $\text{Ni}_2\text{SiO}_4$  due to the incompressibility of the  $\text{SiO}_4$  tetrahedron in comparison to  $\text{NiO}_6$  octahedron.

In the particular case of  $\text{ZnGa}_2\text{O}_4$ , the decrease of  $u$  with pressure is a consequence of the larger polyhedral compressibility of the  $\text{ZnO}_4$  tetrahedra than that of the  $\text{GaO}_6$  octahedra. To understand better the relation between polyhedral compressibility and the pressure evolution of  $u$ , we should remember that the Zn–O and Ga–O bond distances are given by:  $R_{\text{Zn-O}} = \sqrt{3}(u - 0.125)a$  and  $R_{\text{Ga-O}} = \sqrt{(3u^2 - 2u + 0.375)}a$ . This means that at  $u = 0.2625$   $R_{\text{Zn-O}} = R_{\text{Ga-O}}$  and at  $u = 0.25$  the oxygen atoms form a perfect face-centered cubic (fcc) sublattice, being the following relations obtained:  $\partial R_{\text{Zn-O}}/\partial u = \sqrt{3}a$  and  $\partial R_{\text{Ga-O}}/\partial u = -a$ . Thus when  $u$  increases, the tetrahedral bond distances increase while the octahedral bond lengths decrease, and the tetrahedral bond length change faster than the octahedral one. Therefore, upon compression we have two competing effects. On one side, both bond distances tend to decrease because of the reduction of the unit-cell parameter. On the other hand, the reduction of  $u$  contributes to the decrease of the Zn–O distance but partially compensate the decrease of the Ga–O distance (because  $\partial R_{\text{Ga-O}}/\partial u = -a$ ). Thus, Zn–O bonds are expected to be more compressible than Ga–O bonds. This result is in excellent agreement with experimental results summarized in Fig. 2.4. In addition to  $\text{ZnGa}_2\text{O}_4$ , other nice examples to understand the differential bond compressibility of spinels are  $\text{MgAl}_2\text{O}_4$  [34],  $\text{ZnAl}_2\text{O}_4$  [25], and  $\text{Fe}_2\text{SiO}_4$  [33]. The differences in polyhedral compressibilities of different compounds are in good agreement with the predictions of Recio et al. [35]. In particular, these authors show that the bulk compressibility in spinel-type compounds can always be expressed in terms of cation–oxygen polyhedral compressibilities and the pressure effect of the internal oxygen position in the unit cell. This behavior contrast with that of other binary oxide compounds, like zircon or scheelite, where the bulk modulus is mainly controlled by the larger cation polyhedra [36].

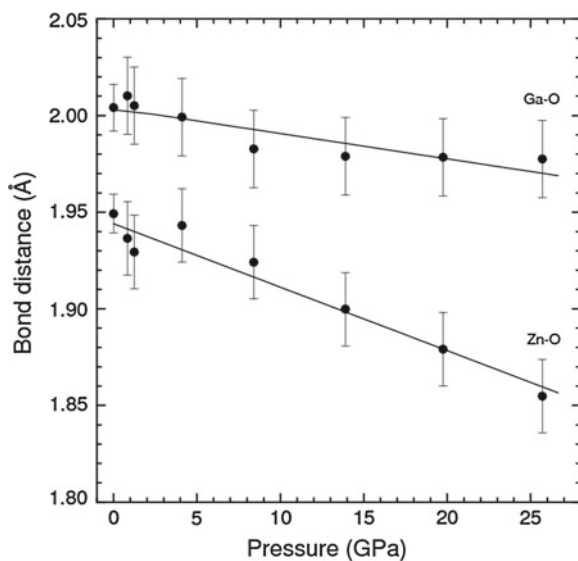


**Fig. 2.4** Bond distances versus pressure obtained from X-ray experiments performed in ZnGa<sub>2</sub>O<sub>4</sub> [4]

## 2.3 High Pressure Phases of Oxospinel

Due to the possible relation of the 660 km seismic discontinuity in the mantle the Earth with pressure-induced changes in (Mg, Fe)<sub>2</sub>SiO<sub>4</sub>, many studies have been carried out examining post-spinel structures. Particular attention has been given to experiments of the transformation of (Mg, Fe)<sub>2</sub>SiO<sub>4</sub> from ringwoodite to (Mg, Fe)O-magnesiowustite and (Mg, Fe)SiO<sub>3</sub>-perovskite. In contrast with this silicate, many AB<sub>2</sub>O<sub>4</sub> spinels have been found to transform to post-spinel structures without decomposition. In particular, the postspinel mineral MgAl<sub>2</sub>O<sub>4</sub> exists under severe pressure conditions in the subducted oceanic lithosphere in the Earth's deep interior. The orthorhombic structures of CaMn<sub>2</sub>O<sub>4</sub> (space group *Pbcm*), CaFe<sub>2</sub>O<sub>4</sub> (space group *Pnma*), and CaTi<sub>2</sub>O<sub>4</sub> (space group *Cmcm*) have been reported as post-spinel phases [6]. Because these structures are very similar, several ambiguities and inconsistencies appear in high-pressure studies. The structures of CaB<sub>2</sub>O<sub>4</sub> (where B = Mn, Fe, Ti) are very similar; distorted BO<sub>6</sub> octahedra sharing edges and corners create a framework, with the Ca<sup>2+</sup> ions occupying one-dimensional six-sided channels coordinated by eight O atoms. CaMn<sub>2</sub>O<sub>4</sub> occurs as the mineral marokite, with highly distorted MnO<sub>6</sub> octahedra, which is due to the strong first-order Jahn–Teller effect of Mn<sup>3+</sup>. Differences between the spinel structure and these three types of structures can be seen in Fig. 2.5. Basically, the atomic arrangements are denser in the high-pressure phases. In fact, cations change their coordination from tetrahedral and octahedral to octahedral and dodecahedral, respectively, during the transformation from the spinel to these high-pressure phases. Consequently, a more compact three

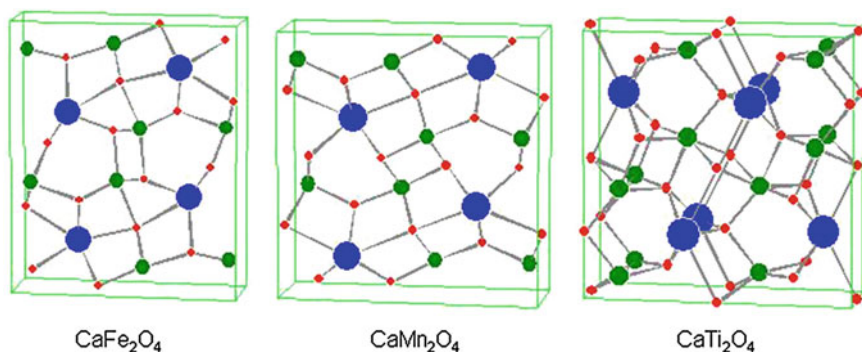


**Fig. 2.5** Schematic view of the orthorhombic post-spinel structures. *Blue spheres*: B cations, *green spheres*: A cations, and *red spheres*: O atoms

dimensional network is formed and consequently the phase transition occurs together with a small volume collapse [18]. The high-pressure phase has also a bulk modulus approximately 25 % larger than the spinel phase [18].

An interesting fact of the transformation to  $\text{CaB}_2\text{O}_4$ -type structures is that it is not only induced by high-pressure experiments. This process has been also discovered to occur naturally, as it was discovered in the Suizhou meteorite [37]. In the laboratory, the transition has been reproduced over a large number of oxides; e.g.  $\text{MgAl}_2\text{O}_4$ ,  $\text{ZnCr}_2\text{O}_4$ ,  $\text{CoFe}_2\text{O}_4$ ,  $\text{CdCr}_2\text{O}_4$ , etc. [38]. A possible mechanism for this post-spinel transformation has been recently proposed [38]. According to it, the transition involves not only simple cation displacements, but also full octahedral movements, which implies a reconstructive transformation. This is likely the reason why phase coexistence is observed in a wide pressure range in many cases [18]. One exception to this rule is natural chromite in which a distortive transition to a  $\text{CaAl}_2\text{O}_4$ -type orthorhombic structure occurs.

An interesting fact to highlight is the existence of an intermediate phase between the cubic spinel and the orthorhombic post-spinel structures in some compounds. This phase is usually a distortion of the cubic structure. A particular compound following this behavior is  $\text{ZnGa}_2\text{O}_4$ . Figure 2.6 shows a series of X-ray powder diffraction patterns collected in  $\text{ZnGa}_2\text{O}_4$  at different pressures and RT. The diffraction patterns can be assigned to the cubic spinel structure up to 31.2 GPa where changes in the diffraction patterns are found. Peaks become much broader and many of them split, as indicated by arrows in Fig. 2.6. This is indicative of the occurrence of a phase transition. Changes become more notorious at higher pressure as can be seen in the spectra recorded at 34.8–48.7 GPa. The changes of the diffraction patterns cannot be explained by any of the known high-pressure post-spinel phases ( $\text{CaFe}_2\text{O}_4$ -,  $\text{CaMn}_2\text{O}_4$ -, and  $\text{CaTi}_2\text{O}_4$ -type). A possible explanation to the experimental results is given by the consideration of the tetragonal spinel structure, the structure of  $\text{ZnMn}_2\text{O}_4$  and  $\text{MgMn}_2\text{O}_4$  [23, 39]. This phase belongs to space group  $I4_1/amd$ , a translationgleiche subgroup of  $Fd\bar{3}m$ . It is formed by a tetragonal



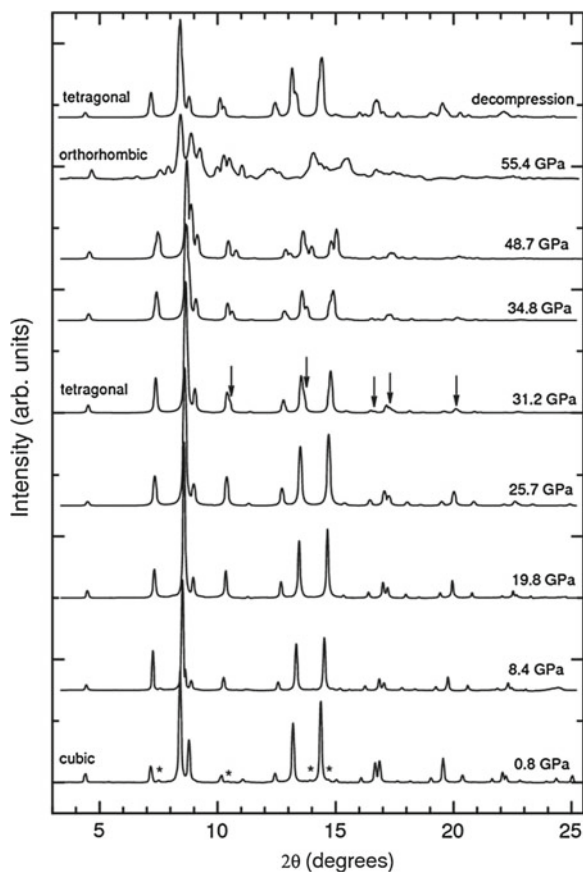


**Fig. 2.6** Selection of XRD patterns collected from ZnGa<sub>2</sub>O<sub>4</sub> at different pressures. Pressures are indicated and characteristic patterns of each phase labeled. The stars indicate impurity peaks assigned to Ga<sub>2</sub>O<sub>3</sub>. The vertical arrows depict the changes associated to the onset of the cubic-tetragonal transition

distortion of the cubic spinel (if in the tetragonal structure  $c/a = \sqrt{2}$  is satisfied, it is reduced to the cubic spinel structure). The cubic-tetragonal transition does not involve any detectable change in the volume. However, upon compression the tetrahedral distortion of the  $I4_1/amd$  structure gradually increases. These facts, and the group-subgroup relationship existent between the cubic and tetragonal phases, point towards the occurrence of a second-order pressure-induced transition in ZnGa<sub>2</sub>O<sub>4</sub>. It is important to note, that the cubic-tetragonal transition has been documented also in NiMn<sub>2</sub>O<sub>4</sub> at 12 GPa [8]. Regarding cation coordination, tetragonal ZnGa<sub>2</sub>O<sub>4</sub> also consists of ZnO<sub>4</sub> tetrahedra and GaO<sub>6</sub> octahedra, but in contrast with cubic ZnGa<sub>2</sub>O<sub>4</sub>, the octahedra are distorted showing four long distances and two short distances.

In  $\text{ZnGa}_2\text{O}_4$  at 55.4 GPa a second transition is detected (see Fig. 2.6). At this pressure, there are important changes observed in the diffraction patterns. The number of diffraction peaks increases considerably in the diffraction patterns, probably as a consequence of a symmetry reduction. In particular, the patterns resemble those of the orthorhombic post-spinel structures of  $\text{MgAl}_2\text{O}_4$  and homologous compounds. In this particular case, the post-spinel phase has a  $\text{CaMn}_2\text{O}_4$ -type structure (marokite) [40]. The transition to the orthorhombic post-spinel structure involves an estimated volume collapse of around 7 %, similar to that observed in other spinels.

Before concluding this section, we would like to mention that high-pressure studies have been also performed on the post-spinel structures. Since these structures are denser than spinel and have a more efficient packing, they are less compressible than spinel. In addition, powder diffraction studies indicated that  $\text{CaMn}_2\text{O}_4$ ,  $\text{CaFe}_2\text{O}_4$ , and  $\text{CaTi}_2\text{O}_4$  have further high-pressure polymorphs [41].  $\text{CaMn}_2\text{O}_4$  transforms to the  $\text{CaTi}_2\text{O}_4$  structure at 30 GPa. Also a new phase was observed at pressures above 50 GPa during compression of  $\text{CaFe}_2\text{O}_4$  [41]. Rietveld refinements demonstrated that the HP structure, with space group  $Pnam$ , is produced via a martensitic transformation by displacing one of every three layers perpendicular to the  $c$  axis.  $\text{CaTi}_2\text{O}_4$  has also a HP polymorphs with space group  $Bbmm$  [41]. Very noticeably is the fact that the transition in  $\text{CaFe}_2\text{O}_4$  is associated to a  $\text{Fe}^{3+}$  spin transition. Single-crystal diffraction measurements have shown that the 50 GPa transition of this compound is isosymmetric, but marked by a 8.4 % volume collapse [42]. X-ray emission spectroscopic data suggest that the transition is related to the  $\text{Fe}^{3+}$  high-spin/low-spin transition. The bulk modulus is remarkably different for the high-spin (159 GPa) and low-spin (235 GPa) structures.

## 2.4 Lattice Vibrations in Spinel

At ambient conditions, the vibrational properties of spinel oxides have been mostly studied with Raman (R) and infrared (IR) spectroscopy but a few studies using inelastic neutron scattering are available [43]. However, high-pressure studies of the lattice dynamics have been mostly performed using Raman spectroscopy. Therefore, in this section we will concentrate on discussing Raman results.

The normal vibrations of a crystal can be determined if one knows its crystalline structure (the primitive unit cell) and applies group theory. To calculate lattice vibrations the full cubic unit cell of spinel is redundant. It contains 56 atoms, but the smallest Bravais cell; i.e., the primitive cell, has only 14 atoms. As a result, one should expect 42 vibrational modes. Group theory analysis predicts the following irreducible representations for the modes at the  $\Gamma$  point of the Brillouin zone [44]:

$$\Gamma = A_{1g}(\text{R}) + E_g(\text{R}) + T_{1g} + 3T_{2g}(\text{R}) + 2A_{2u} + 2E_u + 4T_{1u}(\text{IR}) + T_{1u} + 2T_{2u}$$

where Raman- and infrared-active modes are indicated, and the rest of the modes are acoustic or silent modes. Note that T modes are also noted as F modes in the

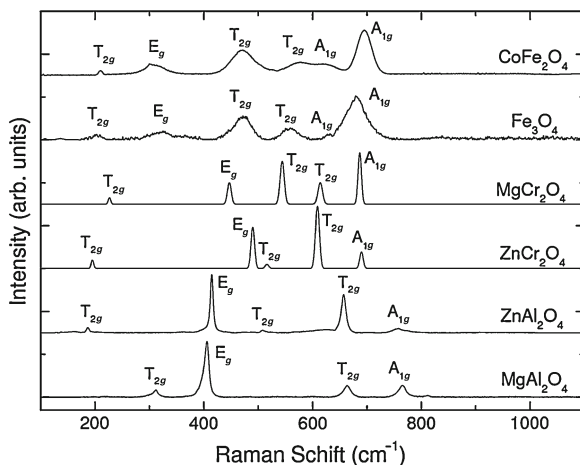


**Fig. 2.7** Selection of ambient conditions Raman spectra of different ABO<sub>4</sub> spinels

literature and that E and T modes are double and triple degenerate, respectively. In normal non-defective spinels selection rules indicate that only five modes should be Raman active and four modes infrared active. Non-stoichiometry, the presence of vacancies, interstitial cations, and defects in general, may result in activation of phonon modes not predicted by group theory.

Figure 2.7 shows a selection of Raman spectra collected from different compounds at ambient conditions. There it can be seen that in MgAl<sub>2</sub>O<sub>4</sub> usually only four of the five allowed modes are observed. A typical feature of all the spectra is that the A<sub>1g</sub> mode is the one with highest frequency. In general, the mode frequencies follow the sequence  $T_{2g} < E_g < T_{2g} < T_{2g} < A_{1g}$ . In addition the lowest frequency T<sub>2g</sub> mode is one of the weakest modes. In the figure, it can be also seen that the Raman spectra of different aluminates resemble very much to each other. The same can be said for chromites and ferrites. These similarities are related to the fact that some Raman vibrations can be associated to internal vibrations of the BO<sub>6</sub> octahedra and AO<sub>4</sub> tetrahedra. It is noticeably in the cases of Fe<sub>3</sub>O<sub>4</sub> and CoFe<sub>2</sub>O<sub>4</sub> the splitting of the high-frequency A<sub>1g</sub> mode. This fact is caused by a partial cation redistribution [45], being the relative intensity ratio between both A<sub>1g</sub> peaks decreasing with lowering of inversion in the spinel structure.

MgAl<sub>2</sub>O<sub>4</sub> has been one of the most studied spinels. Table 2.3 summarizes the theoretical and experimental Raman modes [43, 46–49]. The calculated frequencies agree with the experimental values within 5%. Most experiments found only four Raman modes. Only one experiment [46] reported a fifth mode which is very weak. As the differences in frequency of this mode with the “missing” T<sub>2g</sub> mode is larger than 15% there are doubts about its assignation. In particular, it has been stated that its occurrence could be probably related to cation disorder [43]. Cation disorder is also the cause of the A<sub>1g</sub> mode splitting reported in [46] and [49]. Calculations also agree

**Table 2.3** Frequencies of the Raman modes of  $\text{MgAl}_2\text{O}_4$  at ambient conditions. All frequencies are given in  $\text{cm}^{-1}$

Mode	Theory	Experiments			
		Reference [46]	Reference [47]	Reference [48]	Reference [49]
$T_{2g}$	319	311	311	312	311
$E_g$	426	410	408	407	409
$T_{2g}$		492			
$T_{2g}$	570				
$T_{2g}$	682	671	669	666	670
$A_{1g}$		727			727
$A_{1g}$	776	772	770	767	770

well with experiments regarding IR modes [43]. For these modes, the mode assignment is more complicated than in Raman because the induced macroscopic electric field lifts the threefold degeneracy of IR-active  $T_{1u}$  modes. Consequently, they split into twofold degenerate TO modes and a single LO mode. The TO (LO) modes measured in experiments are 304 (312), 476 (610), 578 (575), and 676(868) $\text{cm}^{-1}$ .

Before discussing pressure effects on Raman modes we will dedicate a few paragraphs to relate atomic motions with Raman modes. The  $A_{1g}$  mode corresponds to a symmetric breathing mode of the  $\text{AO}_4$  tetrahedron [50] where only the oxygen atoms move. Regarding the highest-frequency  $T_{2g}$  mode the literature disagrees. Some authors assign it to an anti-symmetric breathing mode of the  $\text{AO}_4$  tetrahedron and others to an asymmetric bending motion of the oxygens bonded to the A cation [50]. The assignment is clear for the remaining modes [50]. The lowest-frequency  $T_{2g}$  mode is a complete translation of the  $\text{BO}_6$  octahedron against the A cation. The  $E_g$  mode is a symmetric bending motion of the oxygens within the  $\text{AO}_4$  units and

**Table 2.4** Experimental Raman frequencies (in  $\text{cm}^{-1}$ ) for different modes of several  $\text{ABO}_4$  spinels

Spinel	$T_{2g}$	$E_g$	$T_{2g}$	$T_{2g}$	$A_{1g}$	Reference
$\text{MgAl}_2\text{O}_4$	311	409		670	727, 770	[49]
$\text{MgCr}_2\text{O}_4$	227	447	544	614	687	[51]
$\text{MgMn}_2\text{O}_4$	313	313	375	507	666	[52]
$\text{MgFe}_2\text{O}_4$	217	333	486	554	646, 715	[7]
$\text{ZnAl}_2\text{O}_4$	197	417	509	658	758	[53]
$\text{ZnCr}_2\text{O}_4$	180	430, 457	511	605	687	[54]
$\text{ZnMn}_2\text{O}_4$	300	320	381	475	678	[52]
$\text{ZnFe}_2\text{O}_4$	221	246	355	451	647	[51]
$\text{FeAl}_2\text{O}_4$	184		593	701	753	[55]
$\text{FeCr}_2\text{O}_4$					686	[56]
$\text{Fe}_3\text{O}_4$	193	306		538	668	[57]
$\text{MnCr}_2\text{O}_4$		457	511	600	671, 685	[58]
$\text{MnFe}_2\text{O}_4$	189	339	446	559	647	[59]
$\text{Mn}_3\text{O}_4$	300	320	382	475	678	[52]

the remaining  $T_{2g}$  mode is a translation along one direction of the lattice, with the cations and oxygen atoms moving in opposite directions. Summarized in Table 2.4 there are the Raman modes for different compounds to illustrate the influence of cation replacement in them. Clearly the  $A_{1g}$  mode is strongly affected by B cation substitution and the lowest-frequency  $T_{2g}$  mode by A cation substitution.

## 2.5 High-Pressure Raman Scattering Studies

As commented, experimental high-pressure studies of lattice dynamics in oxospinel have been done by using Raman scattering measurements. Table 2.5 summarizes Raman modes and pressure coefficients of different zinc oxospinel. There, it can be seen that among the modes of the spinel phase the two low-wave number modes exhibit pressure coefficients smaller than the other modes. In particular, it is noticeably that the low-frequency  $T_{2g}$  mode, associated to translations of the octahedral BO<sub>6</sub> units, has the smallest pressure coefficient of all modes. Another systematic behavior to stress is that the  $A_{1g}$  high-frequency mode of the ZnO<sub>4</sub> tetrahedral groups tends to have a larger pressure coefficient than the bending modes associated to these groups. The first feature is related to the fact that Zn–O bonds are shorter than the B–O bonds in all spinel oxides. This means that the Zn–O distance is less compressible than the B–O distance; therefore, the low-frequency  $T_{2g}$  mode, which triggers the Zn–O distance, is almost unaffected by compression. The second one suggests that in spinels bond stretching has a larger force constant than bond-bending. A similar systematic behavior than in ZnB<sub>2</sub>O<sub>4</sub> spinels has been found for MgB<sub>2</sub>O<sub>4</sub> spinels [7, 51]. This picture is supported by lattice-dynamics calculations [53, 60]. Similar high-pressure evolutions are also obtained for IR-active modes. In both ZnAl<sub>2</sub>O<sub>4</sub> and ZnGa<sub>2</sub>O<sub>4</sub>, the highest frequency IR mode has  $d\omega/dP > 4 \text{ cm}^{-1}/\text{GPa}$  and the lowest frequency IR modes have  $d\omega/dP < x \text{ cm}^{-1}/\text{GPa}$ . An interesting fact to remark before discussing the Raman modes of high-pressure phases is the not existence of soft modes within the pressure range of stability of the cubic spinel phase in any of the studied compounds. This indicate that the observed pressure-induced transitions

**Table 2.5** Experimental Raman-mode frequencies at ambient conditions ( $\omega$ ) and their pressure dependences ( $d\omega/dP$ ) for ZnBO<sub>4</sub> spinels

Mode	ZnFe <sub>2</sub> O <sub>4</sub>		ZnCr <sub>2</sub> O <sub>4</sub>		ZnAl <sub>2</sub> O <sub>4</sub>		ZnGa <sub>2</sub> O <sub>4</sub>	
	$\omega$ (cm <sup>-1</sup> )	$d\omega/dP$ (cm <sup>-1</sup> /GPa)	$\omega$ (cm <sup>-1</sup> )	$d\omega/dP$ (cm <sup>-1</sup> /GPa)	$\omega$ (cm <sup>-1</sup> )	$d\omega/dP$ (cm <sup>-1</sup> /GPa)	$\omega$ (cm <sup>-1</sup> )	$d\omega/dP$ (cm <sup>-1</sup> /GPa)
$T_{2g}$	221	1.31	180	2.05	196			
$E_g$	246	0.77	430	2.67	417	2.2		
$T_{2g}$	355	4.01	511	4.07	488		465	3.5
$T_{2g}$	451	3.95	605	4.11	658	3.8	608	3.7
$A_{1g}$	647	2.76	692	4.61	758		710	4.4

Data taken from references [11, 51, 53]

are not caused by mechanical instabilities of the spinel phase and occur because high-pressure phases become thermodynamically more stable than the spinel phase upon compression. A final fact to highlight on high-pressure measurements on the low-pressure cubic spinel phase is that the intensities of the Raman bands gradually decrease as pressure approach the phase-transition pressure. In most compounds, the majority of the Raman modes completely disappear before the transition is completed (there is a phase coexistence within a large pressure range). Usually, only the peak resulting from the  $A_{1g}$  mode can be observed continuously up to the completion of the transition. Note that most high-pressure Raman studies were performing using less hydrostatic pressure media than He or Ne. Therefore, the influence of non-hydrostatic stresses in the results cannot be neglected. Future studies carried out under quasi-hydrostatic conditions will probably clarify this issue.

## 2.6 Raman of Post-Spinel Phases

According to group-theory analysis, the tetragonal spinel structure observed in  $\text{ZnGa}_2\text{O}_4$  and other spinels has the following set of Raman-active modes:

$$\Gamma = 2A_{1g} + 3B_{1g} + B_{2g} + 4E_g$$

With the correlation between the modes of the point groups of the cubic and tetragonal structure (remember that the tetragonal group is a subgroup of the cubic), the five modes of the cubic spinel transform into ten modes. In particular, the Raman inactive  $T_{1g}$  mode of the cubic spinel transforms into  $A_{2g} + E_g$  modes. On the other hand, the Raman-inactive  $A_{2g}$  mode of cubic spinel is also inactive in the tetragonal structure. Raman experiments have been carried out in tetragonal  $\text{CoFe}_2\text{O}_4$  [61] and only six modes have been observed. These modes clearly correspond to the splitting of the cubic modes and their pressure evolution is similar. In special, the high-frequency modes have pressure coefficients an order of magnitude larger than the lowest frequency mode, resembling the pressure behaviour of the Raman modes in cubic spinel. Unfortunately, high-pressure Raman studies performed in  $\text{ZnGa}_2\text{O}_4$  did not reached the cubic-tetragonal transition pressure [53]. Extension of these studies could give a quite elegant confirmation of the transition. Raman modes are expected to gradually split as observed in similar (second order) transitions where the low- and high-pressure phases are related by group-subgroup relationships [62].

According to group-theory analysis, the three different orthorhombic post-spinel structures are associated with the following three sets of Raman-active modes:

$$(\text{CaFe}_2\text{O}_4\text{-type}) : \Gamma = 7A_{1g} + 5B_{1g} + 7B_{2g} + 5B_{3g}$$

$$(\text{CaMn}_2\text{O}_4\text{-type}) : \Gamma = 6A_{1g} + 7B_{1g} + 6B_{2g} + 5B_{3g}$$

$$(\text{CaTi}_2\text{O}_4\text{-type}) : \Gamma = 6A_{1g} + 4B_{1g} + 2B_{2g} + 6B_{3g}$$

The  $A_{1g}$  and  $E_g$  modes of the cubic structure transform to the  $A_{1g}$  modes of the orthorhombic structures and the  $T_{2g}$  modes of cubic spinel transform to the  $B_{1g} + B_{2g} + B_{3g}$  modes. The orthorhombic structures have 18 or 24 Raman active modes. However, considerably much less modes have been observed in the experiments from these phases [53]. The reasons for it are not clear yet. One remarkable fact is that in the high-pressure phases the pressure coefficients of the observed mode frequencies are at most around  $3 \text{ cm}^{-1}/\text{GPa}$ , while in the spinel phase coefficients around  $5 \text{ cm}^{-1}/\text{GPa}$  are observed for the high-frequency modes. This behaviour is related to the compressibility decrease of the post-spinel phases (see 2.5). Calculations also predict a similar behaviour [53]. In particular, in post-spinel phases of  $\text{ZnAl}_2\text{O}_4$  and  $\text{ZnGa}_2\text{O}_4$  all Raman-active modes are located between 100 and  $980 \text{ cm}^{-1}$  and pressure coefficients are smaller than  $3.4 \text{ cm}^{-1}/\text{GPa}$  [53]. Again, as in the low-pressure phase, Raman-active soft modes have not been observed in any of the post-spinel structures.

## 2.7 Elastic Constants

The elastic constants of magnesium aluminate spinel have been measured by an ultrasonic technique. The results are  $C_{11} = 279 \text{ GPa}$ ,  $C_{44} = 153 \text{ GPa}$ , and  $C_{12} = 153 \text{ GPa}$  [63]. In the case of  $\text{Mg}_2\text{SiO}_4$  the obtained constants are  $C_{11} = 327 \text{ GPa}$ ,  $C_{44} = 112 \text{ GPa}$ , and  $C_{12} = 126 \text{ GPa}$  [64]. The set of elastic constants calculated fulfil the stability criteria for a cubic crystal:  $(C_{11} - C_{12}) > 0$ ,  $C_{11} > 0$ ,  $C_{44} > 0$ , and  $(C_{11} + 2C_{12}) > 0$ , pointing to their mechanical stability. Similar results have been obtained from Brillouin scattering and theoretical calculations [64]. These constants allow the calculation of the shear ( $G$ ) and bulk modulus ( $B$ ), as well as of the isotropic velocities for shear ( $v_S$ ) and pressure ( $v_P$ ) waves [64, 65]. In the case of  $\text{Mg}_2\text{SiO}_4$  their values are  $B = 185 \text{ GPa}$ ,  $G = 119 \text{ GPa}$ ,  $v_S = 5.77 \text{ km/s}$ , and  $v_P = 9.79 \text{ km/s}$ . The Young modulus,  $E = 293 \text{ GPa}$ , and the Poisson ratio,  $\nu = 0.23$ , of  $\text{Mg}_2\text{SiO}_4$  can be also obtained. In particular, it is observed that the elastic constant anisotropy, the Zener ratio  $A = 2C_{44}/(C_{11} - C_{12})$ , is weak ( $A = 1.04$ ). Additionally, the Zener ratio increases with increasing pressure, reaching 1.06 at pressures close to that of the Earth's transition zone, and subsequently increasing up to 1.09 at 30 GPa. Figure 2.8 shows the typical calculated behaviour for the elastic constants upon compression.

Elastic constants can be used to estimate the hardness and ductility of materials. In the case of spinels, it is usually found that  $B/G$  is smaller than 1.75 which indicates that spinel oxides are brittle materials. This conclusion is consistent with the fact that spinel has a brittleness similar to that of sapphire. Regarding the hardness of spinel, it is known to be 8 in the Mohs scale. Employing the correlation between the shear modulus and the Vickers hardness reported by Teter [66], since most oxospinel have a similar shear modulus, it is possible to conclude that most oxospinel should have a similar hardness than  $\text{MgAlO}_4$ .

The pressure dependence of the sound velocities, single-crystal elastic constants, and shear and adiabatic bulk moduli of a natural gahnite ( $\text{ZnAl}_2\text{O}_4$ ) spinel have

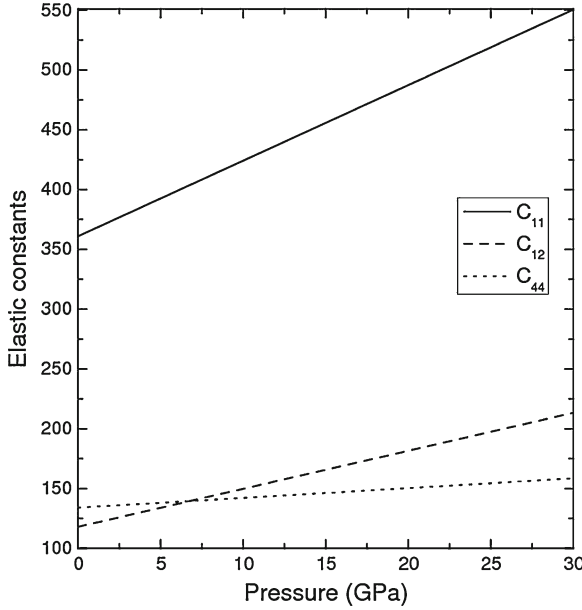


**Fig. 2.8** Pressure evolution of the elastic constants of  $\text{Mg}_2\text{SiO}_4$

been determined to 9 GPa by gigahertz ultrasonic interferometry in a DAC [67]. The elastic constants of gahnite are  $C_{11} = 290$  GPa,  $C_{12} = 169$  GPa, and  $C_{44} = 146$  GPa. The elastic constants  $C_{11}$  and  $C_{12}$  have similar pressure derivatives of 4.48 and 5.0, while the pressure derivative of  $C_{44}$  is 1.47. In contrast to  $\text{ZnAl}_2\text{O}_4$  and the previous described spinels, magnetite exhibits  $C_{44}$  mode softening under pressure.

The elastic constants of  $\text{CoAl}_2\text{O}_4$ , a normal spinel, and  $\text{CoFe}_2\text{O}_4$ , an inverse spinel, have been determined by an ultrasonic method [68]. The measured values are:  $C_{11} = 290.5$  GPa,  $C_{12} = 170.3$  GPa, and  $C_{44} = 138.6$  GPa for  $\text{CoAl}_2\text{O}_4$ , and  $C_{11} = 257.1$  GPa,  $C_{12} = 150.0$  GPa, and  $C_{44} = 85.3$  GPa for  $\text{CoFe}_2\text{O}_4$ . By comparing these constants with the above summarized data and previously published data of other spinel crystals, it can be concluded that the cation valence and cation distribution have little influence on the elastic properties of the spinel materials.

To conclude this section, we would like to mention that recently accurate measurement of elastic constants have been performed in natural chromian spinels (found in mantle xenoliths from Sveyagin, Russia) by high-frequency resonant ultrasound spectroscopy [69]. The elastic constants of this mineral are  $C_{11} = 263.3$  GPa,  $C_{12} = 138.0$  GPa, and  $C_{44} = 123.71$  GPa, respectively. Comparison with elastic constants of  $\text{FeAl}_2\text{O}_4$  and  $\text{FeCr}_2\text{O}_4$  confirms that compositional difference have little influence in the elastic constants.



## 2.8 Miscellaneous

Along this chapter we have described the structural, mechanical, and vibrational properties of spinel oxides and their evolution with pressure. There are many other physical properties that have been extensively studied, but they will not be discussed here. Here we will only briefly mention some interesting recent results that we consider should be highlighted. In this respect, we will describe a few important results on magnetism, which has been extensively studied in magnetic spinels like Fe<sub>3</sub>O<sub>4</sub> and CoFe<sub>2</sub>O<sub>4</sub>. A nice review on the magnetic properties of spinel oxide solutions has been published by Harrison and Putnis [70]. In contrast to magnetism, optical and dielectric properties have been also studied, but little has been done under pressure yet. Consequently, these studies have been not included in this chapter for the sake of brevity. For the same reason, we will not make any comment on spinel nanomaterials and thin films.

Regarding the magnetic properties, probably the most studied compounds are spinel ferrites. They are broadly used in transformer or electromagnetic cores because they have a low coercivity. An interesting fact observed in spinel ferrites is that cation migration is related to changes in the magnetic ordering [71]. Regarding the effects of pressure in magnetization, the magnetic moment is continuously reduced by compression. More interesting is the fact that in Fe<sub>3</sub>O<sub>4</sub> and CoFe<sub>2</sub>O<sub>4</sub>, pressure induces a quenching of magnetism, being the non-magnetic configuration recovered after pressure release [72]. Another interesting phenomenon observed in spinels is highly frustrated magnetism induced by compression [73]. In particular, the structure of spinels makes them unique as a testing ground for the physics of frustration. An interesting topic related to magnetic frustration is the formation of the spin-liquid states. To conclude, we will mention that magnetostriction is another interesting phenomenon observed in spinel ferrites which deserves to be studied under pressure.

## 2.9 Summary

In this chapter we have reviewed the effects of pressure in the structural, mechanical, and lattice-dynamics properties of spinel oxides. The behaviour of different compounds having the spinel structure is summarized and the occurrence of phase transitions described. Particular emphasis on the behaviour of archetypical compounds has been given and the behaviour of post-spinel structures discussed. Furthermore, the elastic constants are discussed. The interest on the high-pressure behaviour of oxospinel is constantly on the rise and therefore soon new results will be added soon to those here summarized. The recent structural studies on Co<sub>3</sub>O<sub>4</sub> which shows that the cubic spinel structure persist up to 42 GPa in spite of the charge transfer induced at lower pressures [74] and the non-monotonic behavior recently observed for the charge gap in ZnV<sub>2</sub>O<sub>4</sub> [75] are only two examples of the permanent progress

done on the study of physical properties of spinels under compression. We hope the results here reviewed will help to trigger new studies to further elucidate the effects of pressure on the properties of spinel and post-spinel compounds [62].

## References

1. Finger LW, Hazen RM, Hofmeister AM (1986) High-pressure crystal-chemistry of spinel ( $\text{MgAl}_2\text{O}_4$ ) and Magnetite ( $\text{Fe}_3\text{O}_4$ ) - Comparisons with silicate spinels. *Phys Chem Minerals* 13:215–220
2. Shim SH, Duffy TS, Shen G (2001) The post-spinel transformation in  $\text{Mg}_2\text{SiO}_4$  and its relation to the 660-km seismic discontinuity. *Nature* 411:571–574
3. Hazen RM, Downs T (eds) (2000) Reviews in mineralogy, vol 41. Mineralogical Society of America, Washington D.C. ISBN 0-939950-53-7
4. Errandonea D, Kumar RS, Manjón FJ, Ursaki VV, Rusu EV (2009) Post-spinel transformations and equation of state in  $\text{ZnGa}_2\text{O}_4$ : Determination at high pressure by in situ X-ray diffraction. *Phys Rev B* 79(6):024103
5. Shim SH, Duffy TS, Shen G (2001) Stability and structure of  $\text{MgSiO}_3$  perovskite to 2300-kilometer depth in Earth's mantle. *Science* 293:2437–2440
6. Ono S, Kikegawa T, Ohishi Y (2006) The stability and compressibility of  $\text{MgAl}_2\text{O}_4$  high-pressure polymorphs. *Phys Chem Miner* 33:200–206
7. Wang Z, Lazor P, Saxena SK, O'Neill HS (2002) High-pressure Raman spectroscopy of ferrite  $\text{MgFe}_2\text{O}_4$ . *Mater Res Bull* 37:1589–1602
8. Asbrink S, Waskowska A, Olsen JS, Gerward L (1998) High-pressure phase of the cubic spinel  $\text{NiMn}_2\text{O}_4$ . *Phys Rev B* 57:4972–4974
9. Greenberg E, Rozenberg GK, Xu W, Arielly R, Pasternak MP, Melchior A, Garbarino G, Dubrovinsky LS (2009) On the compressibility of ferrite spinels: a high-pressure X-ray diffraction study of  $\text{MFe}_2\text{O}_4$  ( $\text{M} = \text{Mg, Co., Zn}$ ). *High Press Res* 29:764–779
10. Yong W, Botis S, Shieh SR, Shi W, Withers AC (2012) Pressure-induced phase transition study of magnesiochromite ( $\text{MgCr}_2\text{O}_4$ ) by Raman spectroscopy and X-ray diffraction. *Phys Earth & Planet Int* 196–197:75–82
11. Wang Z, Lazor P, Saxena SK, Artioli G (2002) High-pressure Raman spectroscopic study of spinel ( $\text{ZnCr}_2\text{O}_4$ ). *J Solid State Chem* 165:165–170
12. Fei YW, Frost DJ, Mao HK, Prewitt CT, Hausermann D (1999) In situ structure determination of the high-pressure phase of  $\text{Fe}_3\text{O}_4$ . *Am Miner* 84:203–206
13. Wittlinger J, Werner S, Schulz H (1997) On the amorphisation of  $\text{ZnCr}_2\text{S}_4$  spinel under high pressure: X-ray diffraction studies. *Phys Chem Miner* 24:597–600
14. Santamaria-Perez D, Amboage E, Manjón FJ, Errandonea D, Muñoz A, Rodriguez-Hernandez P, Mujica A, Radescu S, Ursaki VV, Tiginyanu IM (2012) Crystal chemistry of  $\text{CdIn}_2\text{S}_4$ ,  $\text{MgIn}_2\text{S}_4$ , and  $\text{MnIn}_2\text{S}_4$  Thiospinels under High Pressure. *J Phys Chem C* 116:14078–14087
15. Amiel Y, Rozenberg GK, Nissim N, Milner A, Pasternak MP, Hanfland M, Taylor RD (2011) Intricate relationship between pressure-induced electronic and structural transformations in  $\text{FeCr}_2\text{S}_4$ . *Phys Rev B* 84(9):224114
16. Tang J, Matsumoto T, Furubashi T, Kosaka T, Nagata S, Kato Y (1998) Metal-insulator transition of  $\text{CuIr}_2(\text{S, Se})_4$  under high pressure. *J Magn Magn Mat* 177–181:1363–1364
17. Furubayashi T, Kosaka T, Tang J, Matsumoto T, Kato Y, Nagata S (1997) Pressure induced metal-insulator transition of selenospinel  $\text{CuIr}_2\text{Se}_4$ . *J Phys Soc Japan* 66:1563–1564
18. Wang A, Saxena SK, Zha CS (2002) In situ X-ray diffraction and Raman spectroscopy of pressure-induced phase transformation in spinel  $\text{Zn}_2\text{TiO}_4$ . *Phys Rev B* 66(6):024103 (6)
19. Birch F (1978) Finite strain isotherm and velocities for single-crystal and polycrystalline NaCl at high-pressures and 300° K. *J Geophys Res* 83:1257–1268

20. Levy D, Pavese A, Sani A, Pischedda V (2001) Structure and compressibility of synthetic ZnAl<sub>2</sub>O<sub>4</sub> (gahnite) under high-pressure conditions, from synchrotron X-ray powder diffraction. *Phys Chem Miner* 28:612–618
21. Levy D, Diella V, Pavese A, Dipiaggi M, Sani A (2005) P-V equation of state, thermal expansion, and P-T stability of synthetic zincochromite (ZnCr<sub>2</sub>O<sub>4</sub> spinel). *Am Mineral* 90:1157–1162
22. Levy D, Pavese A, Hanfland M (2000) Phase transition of synthetic zinc ferrite spinel (ZnFe<sub>2</sub>O<sub>4</sub>) at high pressure, from synchrotron X-ray powder diffraction. *Phys Chem Miner* 27:638–644
23. Asbrink S, Waskowska A, Gerward L, Olsen JS, Talik E (1999) High-pressure phase transition and properties of spinel ZnMn<sub>2</sub>O<sub>4</sub>. *Phys Rev B* 60:12651–12656
24. Fan D, Zhou W, Liu C, Liu Y, Jing X, Wan F, Liu J, Li X, Xie H (2008) Thermal equation of state of natural chromium spinel up to 26.8 GPa and 628 K. *J Mater Sci* 43:5546–5550
25. Nestola F, Boffa Ballaran T, Dal Negro A (2010) New accurate compression data for gamma-Fe<sub>2</sub>SiO<sub>4</sub>. *Phys Earth Planet Interiors* 183:421–425
26. Hofmeister AM, Wopenka B, Locock AJ (2004) Spectroscopy and structure of hironite, grossite, and CaAl<sub>2</sub>O<sub>4</sub>: Implications for astronomical environments. *Geochim Cosmochim Acta* 68:4485–4503
27. Wittlinger J, Werner S, Schulz H (1998) Pressure-induced order-disorder phase transition of spinel single crystals. *Acta Cryst B* 54:714–721
28. Hazen RM, Yang H (1999) Effects of cation substitution and order-disorder on P-V-T equations of state of cubic spinels. *Am Mineral* 84:1956–1960
29. Waskowska A, Gerward L, Olsen JS, Talik E (2001) CuMn<sub>2</sub>O<sub>4</sub>: properties and the high-pressure induced Jahn-Teller phase transition. *J. Phys.: Condens. Matter* 13:2549–2562
30. Waskowska A, Gerward L, Olsen JS, Feliz M, Llusar R, Gracia L, Marques M, Recio JM (2004) High-pressure behaviour of selenium-based spinels and related structures - an experimental and theoretical study. *J. Phys.: Condens. Matter* 16:53–63
31. Halevy I, Dragoi D, Üstündag E, Yue AF, Arredondo EH, Hu J, Somayazulu M (2002) The effect of pressure on the structure of NiAl<sub>2</sub>O<sub>4</sub>. *J Phys Condens Matter* 14:10511–10516
32. Bouhemadou A, Khenata R (2006) Pseudo-potential calculations of structural and elastic properties of spinel oxides ZnX<sub>2</sub>O<sub>4</sub> (X = Al, Ga, In) under pressure effect. *Phys Lett A* 360:339–343
33. Nestola F, Balic-Zunic T, Koch. Müller M, Secco L, Princivalle F, Parisi F, Dal Negro A, (2011) High-pressure crystal structure investigation of synthetic Fe<sub>2</sub>SiO<sub>4</sub> spinel. *Miner Mag* 75:2649–2655
34. Nestola F, Ballaran TB, Balic-Zunic T, Princivalle F, Secco L (2007) Comparative compressibility and structural behavior of spinel MgAl<sub>2</sub>O<sub>4</sub> at high pressures: The independency on the degree of cation order. *Am Miner* 92:1838–1843
35. Recio JM, Franco R, Martin Pendas A, Blanco MA, Pueyro L, Pandey R (2001) Theoretical explanation of the uniform compressibility behavior observed in oxide spinels. *Phys Rev B* 63(7):184101
36. Errandonea D, Manjón FJ (2008) Pressure effects on the structural and electronic properties of ABX<sub>4</sub> scintillating crystals. *Prog Mat Sci* 53:711–773
37. Chen M, Shu J, Xie X, Mao HK (2003) Natural CaTi<sub>2</sub>O<sub>4</sub>-structured FeCr<sub>2</sub>O<sub>4</sub> polymorph in the Suizhou meteorite and its significance in mantle mineralogy. *Geochim Cosmochim Acta* 67:3937–3942
38. Arevalo-Lopez AM, Dos Santos-Garcia AJ, Castillo-Martinez E, Duran A, Alario-Franco MA (2010) Spinel to CaFe<sub>2</sub>O<sub>4</sub> Transformation: Mechanism and Properties of beta-CdCr<sub>2</sub>O<sub>4</sub>. *Inorg. Chem.* 49:2827–2833
39. Malavasi L, Tealdi C, Flor G, Amboage M (2005) High-pressure stability of the tetragonal spinel MgMn<sub>2</sub>O<sub>4</sub>: role of inversion. *Phys Rev B* 71(9):174102
40. Giesber H, Pennington WT, Kolis JW (2001) Redetermination of CaMn<sub>2</sub>O<sub>4</sub>. *Acta Cryst C* 57:329–330
41. Yamanaka T, Uchida A, Nakamoto Y (2008) Structural transition of post-spinel phases CaMn<sub>2</sub>O<sub>4</sub>, CaFe<sub>2</sub>O<sub>4</sub>, and CaTi<sub>2</sub>O<sub>4</sub> under high pressures up to 80 GPa. *Am Mineral* 93:1874–1881

42. Merlini M, Hanfland M, Gemmi M, Huotari S, Simonelli L, Strobel P (2010)  $\text{Fe}^{3+}$  spin transition in  $\text{CaFe}_2\text{O}_4$  at high pressure. *Am Mineral* 95:200–203
43. De Wijs GA, Fang CM, Kresse G, de With G (2002) First-principles calculation of the phonon spectrum of  $\text{MgAl}_2\text{O}_4$  spinel. *Phys Rev B* 65(5):094305
44. White WB, de Angelis BA (1967) Interpretation of the vibrational spectra of spinels. *Spectrochim Acta A* 23:985–995
45. Chandramohan P, Srinivasan MP, Velmurugan S, Narasimhan SV (2011) Cation distribution and particle size effect on Raman spectrum of  $\text{CoFe}_2\text{O}_4$ . *J Solid State Chem* 184:89–96
46. O'Horo MP, Frisillo AL, White WB (1973) Lattice-vibrations of  $\text{MgAlO}_4$  spinel. *J Phys Chem Solids* 34:23–28
47. Malezieux JM, Piriou B (1988) Relationship between chemical composition and vibrational behaviour in synthetic and natural spinels investigated by Raman microspectroscopy. *Bull Miner* 111:649–669
48. Chopelas A, Hofmeister AM (1991) Vibrational spectroscopy of aluminate spinels at 1 atm and of  $\text{MgAlO}_4$  to over 200 kbar. *Phys Chem Miner* 18:279–293
49. Cynn H, Sharma SJ, Cooney TF, Nicol M (1992) High-temperature Raman investigation of order-disorder behaviour in the  $\text{MgAlO}_4$  spinel. *Phys Rev B* 45:500–502
50. Verble JL (1974) Temperature-dependent light-scattering of verwey transition and electronic disorder in magnetite. *Phys Rev B* 9:5236–5248
51. Wang Z, O'Neil HSC, Lazor P, Saxena SK (2002) High-pressure Raman spectroscopic study of spinel  $\text{MgCr}_2\text{O}_4$ . *J Phys Chem Solids* 63:2057–2061
52. Malavasi L, Galinetto P, Mozzati MC, Azzoni CB, Flor G (2002) Raman spectroscopy of  $\text{AMn}_2\text{O}_4$  ( $A = \text{Mn, Mg and Zn}$ ) spinels. *Phys Chem Chem Phys* 4:3876–3880
53. Lopez-Moreno S, Rodriguez-Hernandez P, Muñoz A, Romero AH, Manjon FJ, Errandonea D, Rusu E, Ursaki VV (2011) Lattice dynamics of  $\text{ZnAl}_2\text{O}_4$  and  $\text{ZnGa}_2\text{O}_4$  under high pressure. *Ann Phys* 523:157–167
54. Kant C, Deisenhofer J, Rudol T, Mayr F, Schrettle F, Loidl A, Cnezdilov V, Wulferding D, Lemmens P, Tsurkan V (2009) Optical phonons, spin correlations, and spin-phonon coupling in the frustrated pyrochlore magnets  $\text{CdCr}_2\text{O}_4$  and  $\text{ZnCr}_2\text{O}_4$ . *Phys Rev B* 80(10):214417
55. Ospitali F, Sabetta T, Tullini F, Nannetti MC, Di Lonardo G (2005) The role of Raman microspectroscopy in the study of black gloss coatings on Roman pottery. *J Raman Spectrosc* 36:18–23
56. McCarty KF, Boehme DR (1989) A Raman-study of the systems  $\text{Fe}_{3-x}\text{Cr}_x\text{O}_4$  and  $\text{Fe}_{2-x}\text{Cr}_x\text{O}_3$ . *J Solid State Chem* 79:19–27
57. Shebanova ON, Lazor P (2003) Raman spectroscopic study of magnetite ( $\text{FeFe}_2\text{O}_4$ ): a new assignment for the vibrational spectrum. *J Solid State Chem* 31:424–430
58. Taken from the RRUFF database, file R070719
59. Gupta HC, Sinha MM, Balram B, Tripathi BB (1993) A study of the interatomic interaction in oxide spinel  $\text{MnCrO}_4$ . *Physica B* 192:343–344
60. Thibaut P, Gervais F (2002) Ab initio investigation of phonon modes in the  $\text{MgAl}_2\text{O}_4$  spinel. *J Phys Condens Matter* 14:3543–3552
61. Wang Z, Downs RT, Pischedda V, Shetty R, Saxena SK, Zha CS, Zhao YS, Schiefer D, Waskowska A (2003) High-pressure X-ray diffraction and Raman spectroscopic studies of the tetragonal spinel  $\text{CoFe}_2\text{O}_4$ . *Phys Rev B* 68(6):094101
62. Errandonea D, Martinez-Garcia D, Segura A, Haines J, Machado-Charry E, Canadell E, Chervin JC, Chevy A (2008) High-pressure electronic structure and phase transitions in monoclinic  $\text{InSe}$ : X-ray diffraction, Raman spectroscopy, and density functional theory. *Phys Rev B* 77(9):045208
63. Lewis MF (1966) Elastic constants of magnesium aluminate spinel. *J Acoust Soc Am* 40:728–729
64. Kiefer B, Stixrude L, Wentzcovitch R (1997) Calculated elastic constants and anisotropy of  $\text{Mg}_2\text{SiO}_4$  spinel at high pressure. *Geophys Res Lett* 24:2841–2844
65. Errandonea D, Ferrer-Roca C, Martinez-Garcia D, Segura A, Gomis O, Muñoz A, Rodriguez-Hernandez P, Lopez-Solano J, Alconchel S, Sapiña F (2010) High-pressure X-ray diffraction

- and ab initio study of Ni<sub>2</sub>Mo<sub>3</sub>N, Pd<sub>2</sub>Mo<sub>3</sub>N, Pt<sub>2</sub>Mo<sub>3</sub>N, Co<sub>3</sub>Mo<sub>3</sub>N, and Fe<sub>3</sub>Mo<sub>3</sub>N: Two families of ultra-incompressible bimetallic interstitial nitrides. *Phys Rev B* 82(8):174105
66. Teter DM (1998) Computational alchemy: The search for new superhard materials. *MRS Bull* 23:22–27
67. Reichmann HJ, Jacobsen SD (2007) Sound velocities and elastic constants of ZnAl<sub>2</sub>O<sub>4</sub> spinel and implications for spinel-elasticity systematics. *Am Miner* 91:1049–1054
68. Li Z, Fischer ES, Liu JZ, Nevitt MV (1991) Single-crystal elastic constants of Co–Al and Co–Fe spinels. *J Mat Sci* 10:2621–2624
69. Harada Y, Yoneda A, Yamamoto J, Yamazaki D, Yoshino T, Okuchi T, Watanabe T (2011) Report of the Japan Geoscience Union Meeting
70. Harrison RJ, Putnis A (1999) Determination of the mechanism of cation ordering in magnesioferrite (MgFe<sub>2</sub>O<sub>4</sub>) from the time- and temperature-dependence of magnetic susceptibility. *Phys Chem Miner* 26:322–332
71. Yu T, Shen ZX, Shi Y, Ding J (2002) Cation migration and magnetic ordering in spinel CoFe<sub>2</sub>O<sub>4</sub> powder: micro-Raman scattering study. *J Phys Condens Matter* 14:L613–L618
72. Subías G, Cuartero V, Garcia J, Blasco J, Mathon O, Pascarelli S (2009) Pressure-induced magnetic transition in Fe<sub>3</sub>O<sub>4</sub> and CoFe<sub>2</sub>O<sub>4</sub> spinels. *J Phys Conf Series* 190(4):012089 (4)
73. Takagi H, Niihata S (2011) Introduction to frustrated magnetism, Springer series in solid state sciences, Part 3, vol 164. Springer-Verlag Berlin Heidelberg, pp 155–175. ISBN: 978-3-642-10588-3
74. Bai L, Pravica M, Zhao Y, Park C, Meng Y, Sinogeikin S, Shen G (2012) Charge transfer in spinel Co<sub>3</sub>O<sub>4</sub> at high pressures. *J Phys Condens Matter* 24(7):435401
75. Kuntshcer C, Rabia K, Forthaus MK, Abd-Elmeguid MM, Ravadulla F, Kato Y, Batista CD (2012) Nonmonotonic evolution of the charge gap in ZnV<sub>2</sub>O<sub>4</sub> under pressure. *Phys Rev B* 86(5):020405

Pressure-Induced Phase Transitions in AB<sub>2</sub>X<sub>4</sub>  
Chalcogenide Compounds

Manjon, F.J.; Tiginyanu, I.; Ursaki, V. (Eds.)

2014, XIII, 243 p. 121 illus., 33 illus. in color., Hardcover

ISBN: 978-3-642-40366-8